Transactive Control of Electric Railways Using Dynamic Market Mechanisms

David D'Achiardi, Anuradha M. Annaswamy, *Life Fellow, IEEE*, Sudip K. Mazumder, *Fellow, IEEE*, and Eduardo Pilo, *Senior Member, IEEE*

***Abstract*— Electricity demand of electric railways is a relatively unexplored source of flexibility in demand response applications in power systems. In this article, we propose a transactive control-based optimization framework for coordinating the power grid network and the train network. This is accomplished by coordinating dispatchable distributed energy resources (DERs) and demand profiles of trains using a two-step optimization. A railway-based dynamic market mechanism (rDMM) is proposed for the dispatch of DERs in the power network along the electric railway using an iterative negotiation process, generates the profiles of electricity prices, and constitutes the first step. The train dispatch attempts to minimize the operational costs of trains that ply along the railway, while subject to constraints on their acceleration profiles, route schedules, and the train dynamics, and generate demand profiles of trains and constitute the second step. The rDMM seeks to optimize the operational costs of the underlying DERs while ensuring power balance. Together, they form an overall framework that yields the desired transactions between the railway and power grid infrastructures. This overall optimization approach is validated using simulation studies of the Southbound Amtrak service along the Northeast Corridor (NEC) in USA, which shows a 25% reduction in energy costs when compared to standard trip optimization based on minimum work and a 75% reduction in energy costs when compared to the train cost calculated using a field dataset.**

***Index Terms*— Power grid, railway dispatch, renewable integration, social welfare, train dispatch, train network, trajectory optimization.**

I. Introduction

A. Motivation

MODERN electric trains can both demand power from their traction system for locomotion and inject power back into the electricity network through regenerative braking, virtually enabling them to store electricity in the form of kinetic energy [1]. The power profile of a train along a route is in many cases determined by the conductor based on training and experience, attempting to meet a given schedule with little regard to the varying electricity price along the route. In this article, we propose an alternate operation methodology that consists of coordination of train schedules and the dispatch of rail-side distributed energy resources (DERs) and leads to a determination of prices and schedules of power consumption for the trains and power generation for the DERs.

Together, this coordinated operation is shown to minimize the overall electricity cost incurred by the trains. As this coordination occurs through a transactive framework between the train dispatch and the dispatch of railway agents such as DERs, this leads to a transactive control of the two interconnected systems of train network and the power grid network, similar to the transactive controller in [2] and [3]. In addition, this operation methodology accommodates complex traction and train infrastructure ownership structures. This can include systems where multiple train operators traverse tracks owned by various railway operators that can in turn be customers of numerous electric utilities and rail-side DER operators.

B. Literature Review

Related work that has addressed trip optimization in rail networks can be found in [4], [5], [6], [7], and [8]. Wang *et al.* [4] provided a summary of the trajectory planning problem in railway systems. Optimal trajectory planning for electric railways can be found in [5, Ch. 3 and 4], where pseudospectral methods are used to determine optimal railway operation based on models of train dynamics. This work builds upon the work minimization literature developed in [6] and [7]. Finally, Eldredge and Houpt [8] developed a control system to reduce fuel use in freight locomotives. In all of these lines of research, the overall objective is to minimize energy use or work done by the train, rather than the cost of the electricity to the infrastructure manager, an important component of our proposed scheme.

A major driver that allows the proposed transactive coordination framework between the train network and the power network is the transformation of the latter in recent years. This has been due to the explosive growth of renewable energy sources [9] and demand response [10], collectively denoted as DERs. The increasing footprint of these resources enables

Manuscript received 22 May 2021; revised 16 January 2022 and 17 June 2022; accepted 27 July 2022. Date of publication 21 September 2022; date of current version 23 February 2023. This work was supported by the Cyber-Physical Systems Program of NSF under Award 1644877 and Award 1644874. Recommended by Associate Editor N. Quijano. *(Corresponding author: David D'Achiardi.)*

David D'Achiardi and Anuradha M. Annaswamy are with the Department of Mechanical Engineering, Massachusetts Institute of Technology, Cambridge, MA 02139 USA (e-mail: davidhdp@mit.edu; aanna@mit.edu).

Sudip K. Mazumder is with the Department of Electrical and Computer Engineering, University of Illinois at Chicago, Chicago, IL 60607 USA (e-mail: mazumder@uic.edu).

Eduardo Pilo is with the Polytechnic School, Universidad Francisco de Vitoria, 28223 Madrid, Spain (e-mail: eduardo.pilo@ufv.es).

Color versions of one or more figures in this article are available at https://doi.org/10.1109/TCST.2022.3202171.

Digital Object Identifier 10.1109/TCST.2022.3202171

them to be dispatchable and to enter into a transactional framework where incentive information (pricing) and commitment decisions (quantity) can be iteratively exchanged and arrived at an optimal solution. This iterative transactional framework is denoted as dynamic market mechanisms (DMMs) and has been explored in [11], [12], [13], and [14]. The origins of transactive control are very much rooted within the energy application realm, as the ideas of using an incentive signal to alter the behavior of demand-side customers in power systems can be traced back to Schweppe *et al.*'s paper [3] on homeostatic utility control. A large-scale demonstration of this concept can be found in [2] where electric systems with high renewable adoption were considered and shown to meet demand reduction objectives. The DMM-related results in [11] show that DERs can engage in market transactions at the tertiary control level and ensure grid objectives through a hierarchical framework, with asymptotic stability, which results in convergence within a region of attraction. Exactly, how these market mechanisms can be integrated into a real-time market and a regulation market together with secondary control-based automatic generation control (AGC) was explored in [14]. Focus was placed on demand response compatible assets in [12], which provides sufficient conditions for convergence. The implications of DMM in the context of a combined heat and power microgrid were explored in [15] and [16].

Key differences with other demand response applications are tied to the spatiotemporal constraints of the overall grid-railway optimization problem. Other DR applications are posed with assets that are spatially constant, whereas trains enter and depart area control centers (ACCs) tied to the electric infrastructure that powers them. From the optimization lens, the force balance constraint of train dispatch introduces a conservation equation that is not common in DR.

C. Contributions and Article's Organization

In this article, we will enable the coordination of various DERs in a power network that is located along the railway network through the use of a DMM and denote it as railway-based DMM (rDMM). The main challenge in the design of the proposed transactive framework is to coordinate the objectives of the two networks. The points of intersection between these two networks are the need to optimize operational costs and the need to ensure physics-based constraints such as power balance, capacity and operational limits, and train kinematics. A combined optimization problem subject to all underlying constraints can be posed and used to determine the train schedules and prices but can prove to be quite intractable due to the complex nature of the constraints, space- and time-dependent constraints with various intractable coupling mechanisms. We, therefore, adopt a two-step approach where the first consists of railway dispatch of schedules and electricity prices for a given train-demand profile, and the second consists of train dispatch, which determines the train schedules for a given electricity-price profile.

The railway dispatch determines, along each section of the track, the electrical output of each generator, the output of all storage assets, and the output of all cogeneration assets for a given set of profiles of power demand from trains and renewable generation. The train dispatch solves the trajectory optimization problem, i.e., the velocity profiles of the trains, through an energy cost minimization subject to acceleration limits and kinematic constraints. Our thesis in this article is that such a two-step optimization can enable effective coordination between the power grid network and the railway network. In particular, we will show that the two-step optimization will lead to a significant reduction in energy costs through simulation studies. While the methods utilized for solving this two-step optimization are fairly straightforward, the main contribution of this article lies in the novelty of the proposed approach for trip optimization in electric railway networks. The second contribution of this article is a demonstration through a case study of the Amtrak service along the Northeast Corridor (NEC) in USA and composed of multiple sections and DER topologies. To our knowledge, such a transactive approach, which can be viewed as demand response using the flexibility in power consumption of trains, has not been suggested thus far in the literature except for [17] and [18], where we presented preliminary results using this approach.

The remainder of this article is organized as follows. Section II describes the problem faced by the railway and train operators in scheduling DERs and trains along the railway system. In Section III, we break out the railway dispatch, i.e., dispatch of the generators and other assets along the railway track based on the estimated renewable generation, traction electric demand, and electric and thermal loads for each section of the electric railway. Section IV establishes the dynamic model of an electric train and formulates the energy cost minimization problem that needs to be solved by each train traveling along the electric railway. Section V describes the integrated transactive control methodology that iterates between the railway dispatch and the train dispatch solutions to determine the price signals and corresponding dispatch profiles of the agents and trains that minimize the operational costs of the entire system. Section VI presents a case study of the Amtrak service and validates the proposed transactive controller. Realistic accommodation of data has been carried out in this case study, including incorporation of the actual electricity prices from the wholesale market, actual load profiles, realistic train data, and renewable energy profiles available in the public database. Using this case study, we compare our approach with both the current train profile using field data and an optimization framework based on minimization of work. The concluding remarks and future research extensions are discussed in Section VII.

II. Problem Formulation

Electric railway systems can be owned and operated by multiple parties. In some systems, the track and electric system that powers the trains are owned by an entity that charges a fee for the utilization of their facilities. This entity is typically responsible for the maintenance of the track, procuring the electric power to feed the trains, dispatching rail-side DERs, and controlling traffic along the system. These entities are

commonly known as railway operators. We will denote train operators as those who are in charge of the use of the track based on their projected train schedules, maintain and dispatch the trains, and pay usage fees to the various railway operators along the tracks used by their trains. The problem that we consider in this article is a combined optimization of both the railway dispatch and the train dispatch, with railway operator and train operator acting as the interface between the grid network and the train network (see Fig. 4 for an overall schematic).

In Section II-A, we will discuss how railway operators procure electricity and thermal energy from wholesale energy markets, distribution operators (i.e., utility companies), and DERs. In Section II-B, we formulate the underlying optimization problem where the cost is social-welfare-like and depends on the costs incurred by the DERs, the electrical and thermal loads of the railway system, and the electric trains. The resulting solution will then provide optimal profiles for various generation assets as well as the train consumption/generation profiles, i.e., the railway dispatch and the train dispatch. Deriving such a solution, however, proves exceedingly difficult to solve due to the presence of several dynamic nonlinear constraints and the fact that the timescale required to solve the trajectory optimization problem needs to approach real time, especially for the train dispatch. This motivates the two-part solution proposed in Sections III–V.

A. Traction System Preliminaries

A wide range of traction system architectures and technologies have been developed for electrified railway systems, across low frequency (dc, 16.6, 20, and 25 Hz) as well as industrial frequency (50 and 60 Hz) networks that are powered by overhead and third rail traction distribution systems. In addition, electric trains have been both powered by rail-side generators as well as grid-tied systems. In some scenarios, electrical connections to a large-scale electricity distribution or transmission system are complemented with distribution lines that travel along the rail and can be designed such that they improve the reliability of the traction system by providing redundant power supplies to the traction substations feeding the traction system. These various architectures have a direct impact on the flexibility of the demand of the train and therefore a possible energy cost reduction.

A typical architecture of energy procurement and dispatch that occurs along the electric railway is shown in Fig. 1 and will be adopted for the discussions in this article. This architecture is typically adopted in deregulated electricity markets such as Amtrak in the Northeastern United States and will be used in the case study presented in Section VI, that is, we assume that railway operators face delivery charges as distribution-level customers of the various electric utilities that own and operate the distribution systems that feed railway facilities. However, due to the energy requirements and the regulatory setting in which electric railways procure energy, railway operators could access wholesale markets for electricity supply. In addition, we assume that third parties could invest in rail-side DERs, seeking to provide energy services to the railway operator. Competitive retail sales of electricity from power marketers [19] and on-site power purchase agreements (PPAs) offered by Energy Services COmpanies (ESCOs) [20] are both established and growing energy procurement mechanisms for commercial companies, including electric railways.

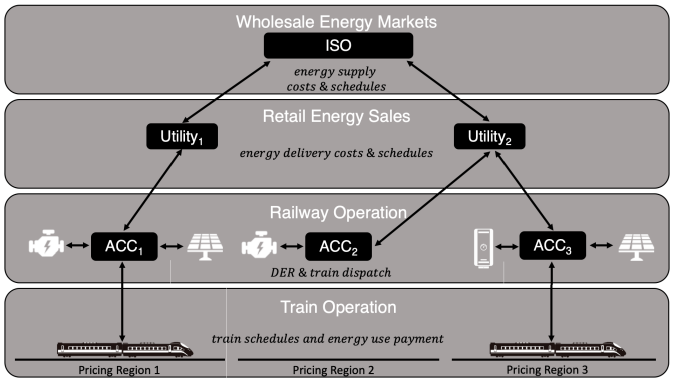

Fig. 1. Summary of the existing activities (power, cost, and information flows) between the four entities (wholesale energy markets, retail energy sales, railway dispatch, and train dispatch) to power within the electric railway network.

B. Overall Constrained Optimization Problem

With the architecture chosen as in Fig. 1, we now introduce a problem formulation for energy procurement and dispatch for optimal grid-railway interaction. A first component of this problem formulation is the ACCs (see Fig. 1) managed by railway operators. An ACC is charged with serving the electric railway traction system, limited to a portion of contiguous electric railway with the property that marginal injections or demands for power have the same cost to the operator for all time t. Along this portion of the track, all rail-side DERs and trains that interface with the traction system are enabled to provide price and quantity information regarding their dispatch and are compensated and charged based on their actions by the ACC. A railway operator manages each ACC with the objective of reducing overall operational costs while maximizing the value of the DERs along the track and meeting all thermal and electric loads in the system, that is, the overall objective of the railway dispatch is to schedule energy resources, which includes trains, so as to minimize the cost of energy resources and trains along the railway system. Such an optimization has to be carried out subject to the various constraints of the grid and railway networks.

More formally, the underlying problem is the dispatch of electric railway power systems across N ACCs in an optimal manner. This includes the electric traction loads of L_n trains, with power profiles denoted as $P_n^l(\tau_n^l)$ for the electric profile of train l in ACC_n over the time interval $\tau_n^l \in [t_{n,0}^l, t_{n,f}^l]$. The railway operator is charged for its electric loads at a rate $\lambda_n(t)$.

On the generation side, we consider D_n dispatchable generators (including DERs and electric utility imports) at each ACC_n with electric and thermal power profiles $P_n^{d_e}$ and $P_n^{d_{\text{th}}}$. For compactness, we will use P_n^d, a tuple of the electric and thermal generation for each generator d. Dispatchable agents

incur a cost $C_n^d(P_n^d)$, which is private to their owner and operator.

All other electric and thermal power demand in the electric railway system, such as the thermal conditioning and lighting loads at passenger stations, are considered price-inelastic and are included within the power balance constraints of the problem for each ACC_n as P_n^e and P_n^{th} but are not included in the objective function due to their fixed nature.

Given that the utility of the trains and generators is fixed, the social welfare maximization problem, which is commonly used for economic dispatch problems in power grids, reduces to a cost minimization problem with two terms in the objective function, the generator cost of generating the electricity and the energy cost of operating the trains.

With the above definitions, the overall grid-railway optimization can thus be posed

$$\min_{U_n \forall n \in \{1,\ldots,N\}} \sum_{n=1}^{N}\left(\sum_{d=1}^{D_n} C_n^d\left(P_n^d\right) + \sum_{l=1}^{L_n}\int_{t_{n,0}^l}^{t_{n,f}^l} P_n^l(\psi)\lambda_n(\psi)d\psi\right) \tag{1}$$

$$\text{s.t.} \sum_{n=1}^{N}\left(\sum_{d=1}^{D_n} P_n^{d_e} + P_n^e\right) + \sum_{l=1}^{L_n} P_n^l = 0 \tag{2}$$

$$\sum_{n=1}^{N}\left(\sum_{d=1}^{D_n} P_n^{d_{\text{th}}} + P_n^{\text{th}}\right) = 0 \tag{3}$$

$$\underline{P_n^d} \le P_n^d \le \overline{P_n^d} \tag{4}$$

$$m_l\ddot{x}_l + F_{\text{DF},l}(\dot{x}_l) + m_l g\sin(\alpha_l(x_l)) = F_{T,l}\left(\frac{P_l}{\dot{x}_l}\right) \tag{5}$$

$$\underline{P_l}(x_l) \le P_l \le \overline{P_l}(x_l) \tag{6}$$

$$\underline{F_{T,l}}(\dot{x}_l) \le F_{T,l} \le \overline{F_{T,l}}(\dot{x}_l) \tag{7}$$

$$\underline{a_l} \le \ddot{x}_l \le \overline{a_l} \tag{8}$$

$$\underline{v_l}(x_l) \le \dot{x}_l \le \overline{v_l}(x_l) \tag{9}$$

$$t_{l,a}(s) \ge \underline{t_l}(s), \quad t_{l,d}(s) \le \overline{t_l}(s) \quad s \in \{0,\ldots,D\} \ge B_F \tag{10}$$

where U_n is a decision variable set that includes $P_n^D = \{P_n^d \forall d \in \{1,\ldots,D_n\}\}$, $P_n^T = \{P_n^l(\tau_n^l) \forall l \in \{1,\ldots,L_n\}\}$, λ_n and $\tau_n = \{\tau_n^l \forall l \in \{1,\ldots,L_n\}\}$. It is clear that the objective function in (1) is composed of the sum of the cost of the dispatchable generators (which we will denote as agents) and the energy expenses of the electric trains. These two costs are the fundamental building blocks of the two-part rDMM developed in Sections III–V. When broken down into the individual ACCs, the first term captures the railway dispatch problem with fixed loads, subject to constraints (2)–(4), which represent nodal electric power balance, nodal thermal balance, and DER agent capacity limits, respectively. The notation and intricacies of each constraint are fully defined in Section III. The second term corresponds to the train dispatch problem, subject to constraints (5)–(10), which represent train dynamics, electric motor power limits, traction force limits, acceleration limits, velocity limits, and schedules, respectively. The notation and intricacies of each term are fully defined in Section IV.

The optimization problem as in (1)–(10) is difficult to solve, highly intractable, and poses several challenges. We note that in the decision variables in the constrained optimization problem in (1)–(10) include power profiles P_n^D of the dispatchable agents, which is a standard feature in optimization problems in power systems. It should be noted that there are additional decision variables, which correspond to the power-demand profiles of trains, P_n^T, and the price of electricity, λ_n, both of which vary with the nth ACC. The final and the most important point to note is that the set of decision variables also includes τ_n, which corresponds to the time intervals during which the trains traverse each of ACC_n. It is clear that there is further coupling between these additional decision variables, as the power profile P_n^l directly affects the absolute time instances at which train l traverses all of the jth ACC, $j \in \{n+1,\ldots,N\}$. In addition, this coupling is nonlinear and highly complex. It is clear, however, that all these quantities, P_n^D, P_n^T, λ_n, and τ_n $\forall n \in \{1,\ldots,N\}$, are all decision variables that affect the overall cost and therefore have to be included simultaneously.

The second challenge introduced by the optimization problem is that its solution requires that all of the traction system agents share their private cost information $C\left(P_n^d\right)$ to appropriately capture and minimize the overall system cost. This feature would likely inhibit private investment in rail-side DERs. The timescale of electric train dispatch may not individually align with that of the ACC_n dispatch. Trajectory optimization of electric railway power profiles occurs in the seconds' timescale, whereas energy asset dispatch is unlikely to be used at a timescale faster than 5 min. Most critically, the trains are entering and exiting each of the ACC_n values at different times that are dependent on the pricing signal.

All of the above challenges make the problem almost intractable since they introduce nonlinearities of various kinds, including an intricate coupling between spatial and temporal constraints. In order to make the problem more tractable, we propose a two-step approach that iterates between the electric railway's minimum cost dispatch problem with fixed train power profiles solved at each ACC_n and the train dispatch problem solved for each electric train under fixed power prices. As will become evident in Sections III–V, such a two-step approach will help decouple some of the interdependencies between various decision variables and the coupling of timescales.

III. Electric Railway Dispatch

This section describes the minimization of energy asset costs in an electric railway where the railway operator must guarantee that all electric and thermal constraints must be met. We will explicitly accommodate the constraints and timescales of each energy agent along the railway. Both thermal and electrical energy assets powering the electric railway are included in this optimization. Section III-A describes the different agents that operate in the system and introduces the timescales in which the agents interact. Section III-B discusses the model used for agent costs and operations within the

railway dispatch problem. Finally, Section III-C uses the agent costs and operations to state and solve the railway dispatch problem, following a similar procedure as the one developed in [15] and [16].

A. Agent Types and Timescales

Within each of the railway segments n, the railway operator must meet the electrical and thermal demand or load during the next M future dispatch intervals that are indexed as $K \in \{1, \ldots, M\}$. Moreover, in managing the electrical system of the railway, the railway operator is tasked with dispatching and compensating the electrical agents or assets within ACC_n in a way that minimizes the total cost of the operation. The electric railway dispatch problem described in this section determines optimal dispatch for each future time interval; however, the pricing and dispatch are only binding and executed for $K = 1$ after the railway dispatch problem has been solved.

We define five types of dispatchable agents within the railway power system at each node n that are classified into the following sets: heating assets (e.g., boilers) $\mathcal{H}_n$, electric generation assets (e.g., fuel cell and microturbines) $\mathcal{E}_n$, cogeneration assets (e.g., combined heat and power units) $\mathcal{C}_n$, storage assets (e.g., batteries) $\mathcal{S}_n$, and low-voltage-side network connections (i.e., points of common coupling) $\mathcal{N}_n$. The set of all dispatchable agents at node n is denoted as $\mathcal{A}_n \triangleq \mathcal{H}_n \cup \mathcal{E}_n \cup \mathcal{C}_n \cup \mathcal{N}_n$. It is assumed that within each dispatch interval K, there are two faster timescales, where the first corresponds to instances $j \in \{1, \ldots, j^{**}\}$, at each of which forecast updates of all nondispatchable loads and generation are received. Between each $[j, j+1]$, we introduce a faster timescale $k \in \{1, \ldots, k^*\}$ where, at each instance k, all dispatchable agents negotiate electric and thermal generation schedules and prices (see Fig. 2). It is assumed that these timescales with j^{**} and k^* are such that they are nested and that the time intervals permit useful forecast data and sufficient negotiations.

In addition to the above agents, we also consider three types of nondispatchable agents at each node n, classified into the following sets: renewable generators, re_n; electrical loads (e.g., lighting at the passenger station), e_n; and thermal loads (e.g., heating of the passenger stations), th_n. The set of these nondispatchable agents at node n is denoted as $\mathcal{F}_n \triangleq \text{re}_n \cup e_n \cup \text{th}_n$, all of whom inject and demand electric and thermal energy from the same network as the dispatchable agents but are not dispatched by the railway operator. Instead, the operators in charge of each of these passive resources (i.e., the renewable asset operator for re_n and the passenger station operator for e_n and th_n) communicate the best load estimate over ACC_n's future time intervals K. This forecast update occurs every j when new updates arrive for the renewable assets or any of the loads. The periods associated with the timescales k and j need to be such that they should accommodate new information related to the forecast and, at the same time, the convergence rates of the negotiations.

Finally, we consider electric trains $l \in \{1, \ldots, L\}$ injecting and demanding electric power from ACC_n. We denote the set of all trains at node n as $\mathcal{T}_n$. For the purpose of the railway dispatch problem, the trains are no different from the set of passive agents $\mathcal{F}_n$ in which the train's electric power profile is updated for the dispatch intervals $K \in \{1, \ldots, M\}$ at each forecast instance j. However, as shown in the following, once we define the train dispatch problem faced by the train operators for each train in Section IV and the composition of the transactive controller in Section V, the train update will transform from a simple forecast update to a price-dependent minimum cost dispatch update.

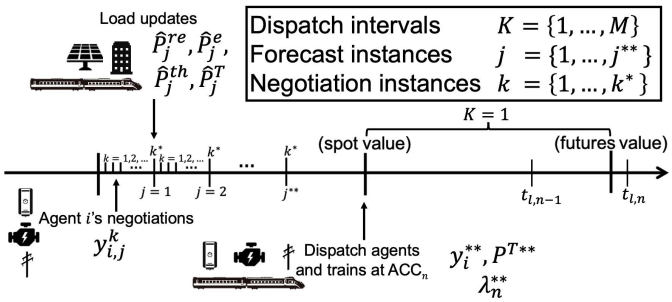

Fig. 2. Timescales within the railway dispatch problem. Dispatch intervals $K \in \{1, \ldots, M\}$ constitute the rolling dispatch horizon considered by the railway operator of ACC_n. The passive agents $\mathcal{F}_n$ and electric trains $\mathcal{T}_n$ provide a thermal and electric load forecast for each dispatch interval during forecast instances $j \in \{1, \ldots, j^{**}\}$. Active agents $\mathcal{A}_n$ negotiate price and quantity during each negotiation instance $k \in \{1, \ldots, k^*\}$ based on the forecast updates and their private cost information. It is assumed that train l traverses ACC_n over the period $[t_{l,n-1}, t_{l,n}]$, which overlaps with the forecast intervals $K = 1$ and $K = 2$.

B. Agent Costs and Operation

The overall goal of railway dispatch is to arrive at pricing information that can yield optimal setpoints for generators and utility power import. Over the time horizon of M dispatch intervals, the electric and thermal power profiles for each of the agents considered (dispatchable, nondispatchable, and trains) are assumed to take positive (generation) and negative (load) values.

In order to capture the electric and thermal components of generation for dispatchable agents in $\mathcal{A}_n$ at each time period M, the output of the generators is denoted by the decision variable

$$y_i \in \mathbb{R}^M \qquad \forall\, i \in \mathcal{A}_n \tag{11}$$

and the Kth element of y_i as $y_{i,K}$. This decision variable maps to an electric and a thermal output as given by

$$g_i^e(y_i) = d_i^e y_i \qquad \forall\, i \in \mathcal{A}_n \tag{12}$$

and

$$g_i^{\text{th}}(y_i) = d_i^{\text{th}} y_i \qquad \forall\, i \in \mathcal{A}_n. \tag{13}$$

In other words, y_i is a dispatch setpoint associated with a particular electric and thermal output. For electric-only generator i, the thermal conversion coefficient vector, $d_i^{\text{th}} \in \mathbb{R}^M$, is the zero vector and the electric conversion coefficient vector, $d_i^e \in \mathbb{R}^M$, takes positive values. We make the following assumptions regarding the constraints and costs of dispatchable agents.

Assumption 1: Electric and thermal power capacities of agent i are bound by $\{\underline{P_i^e}, \overline{P_i^e}\}$ and $\{\underline{P_i^{\text{th}}}, \overline{P_i^{\text{th}}}\}$, respectively.

Assumption 2: Capacity constraints are not binding and losses are negligible for all electrical and thermal equipment in the system other than the dispatchable agents.

Assumption 3: The cost function of each dispatchable agent $i \in A_n$ is a convex quadratic function, as is commonly derived when fitting second-order models to fuel input-power output data from generation units [21].

For a single dispatch interval $K \in \{1, \ldots, M\}$, this quadratic cost is denoted as

$$J_{i,K}(y_{i,K}) = a_{i,K} + b_{i,K} y_{i,K} + \frac{1}{2} c_{i,K} y_{i,K}^2 \tag{14}$$

and over the multiperiods as

$$J_i(y_i) = \sum_{K=1}^{M} J_{i,K}\left(y_{i,K}\right) \qquad \forall i \in \mathcal{A}_n. \tag{15}$$

For the agents representing low-voltage-side network connections $\mathcal{N}$, the cost function can be updated as a function of the equilibrium price in an external market, such as a wholesale energy market. Labeling the external market price for the low-voltage-side network connections as $\pi_{n,j}^{\mathcal{N}}$, the cost function parameters $a_{i,K}$, $b_{i,K}$, and $c_{i,K}$ in (14) are determined for $i \in \mathcal{N}$ at each forecast instance j. Given that these market prices commonly represent marginal prices, the cost function parameters may be simply chosen as: $a_{i,K} = 0$, $b_{i,K} = \pi_{n,j}^{i}$, and $c_{i,K} = 0$.

Each of the passive agents in $\mathcal{F}_n$ determines their power output for the dispatch intervals $K \in \{1, \ldots, M\}$ at each forecast instance j (see Fig. 2), which are denoted by $\hat{P}_{j,K}^{\text{re}}$ for renewable generators, $\hat{P}_{j,K}^{e}$ for electric loads, and $\hat{P}_{j,K}^{\text{th}}$ for thermal loads. We drop the subscript K to denote the power output vector over the dispatch intervals in $\mathbb{R}^M$ as $\hat{P}_j^{\text{re}}$, $\hat{P}_j^{e}$, and $\hat{P}_j^{\text{th}}$. In order to determine the train demand, suppose that train l traverses ACC_n over the period $[t_{l,n-1}, t_{l,n}]$ over the dispatch interval K and $P_l(t, n)$ is the corresponding forecast demand at instance j, and we denote this demand as $P_{l,j,K}^{*}$. This in turn can be summed over all L trains to yield

$$\hat{P}_{j,K}^{T} = \sum_{l=1}^{l=L} P_{l,j,K}^{*}. \tag{16}$$

For ease of exposition, we drop the subscript K in (16) and simply denote the total train demand at forecast instance j as $\hat{P}_j^T$.

C. Railway Dispatch Algorithm

With the overall costs and constraints related to all agents specified as above, we state the railway dispatch problem at ACC_n at a fixed forecast instance $j \in \{1, \ldots, j^{**}\}$ over the dispatch intervals $K \in \{1, \ldots, M\}$ in $\mathbb{R}^M$ as

$$\min_{y_{i,j}\ \forall\, i \in \mathcal{A}_n} \sum_{i \in \mathcal{A}_n} J_i(y_{i,j}) \tag{17}$$

$$\text{s.t. } c_e = \hat{P}_j^{\text{re}} + \hat{P}_j^{T} + \hat{P}_j^{e} + \sum_{i \in \mathcal{A}_n} g_i^{e}(y_{i,j}) = 0 \tag{18}$$

$$c_{\text{th}} = \hat{P}_j^{\text{th}} + \sum_{i \in \mathcal{A}_n} g_i^{\text{th}}(y_{i,j}) = 0 \tag{19}$$

$$m_i^{+}(y_{i,j}) = y_{i,j} - \overline{y_{i,j}} \le 0 \tag{20}$$

$$m_i^{-}(y_{i,j}) = \underline{y_{i,j}} - y_{i,j} \le 0. \tag{21}$$

The output values for each dispatchable agent $i \in \mathcal{A}_n$ over the dispatch interval $K \in \{1, \ldots, M\}$ at dispatch instance j are denoted as $y_{i,j} \in \mathbb{R}^M$ and constitute the decision variables of the problem. These decision variables are bound at each dispatch interval K by the sum of the electric loads per (18), the thermal loads per (19), the maximum capacity constraint per (20) where $\overline{y_{i,j}} = \min\{\overline{P_i^e}/d_i^e, \overline{P_i^{\text{th}}}/d_i^{\text{th}}\}$, and the minimum capacity constraint per (21) where $\underline{y_{i,j}} = \max\{\underline{P_i^e}/d_i^e, \underline{P_i^{\text{th}}}/d_i^{\text{th}}\}$.

At each forecast instance $j \in \{1, \ldots, j^{**}\}$, the power profile for each renewable generator, $\hat{P}_j^{\text{re}} \in \mathbb{R}^M$, electric load, $\hat{P}_j^{e} \in \mathbb{R}^M$, thermal load, $\hat{P}_j^{\text{th}} \in \mathbb{R}^M$, and the total traction load, $\hat{P}_j^{T} \in \mathbb{R}^M$, are updated for the dispatch interval $K \in \{1, \ldots, M\}$. The new forecasts are used to update constraints (18) and (19), with the resulting optimization problem in (17)–(21) solved again.

With each forecast update $j = j + 1$, the decision variables of the problem, denoted as $y_{i,j}^{*}$, optimize the cost in (17). For the dispatch intervals $K \in \{1, \ldots, M\}$, these decision variables can in turn be mapped to the electric and thermal output of the agents as $[g_i^e(y_{i,j}^{*}), g_i^{\text{th}} y_{i,j}^{*})] \in \mathbb{R}^M$.

The underlying optimization problem that the railway operator has to solve is therefore given by the solution of (17)–(21) for a given set of forecast profiles. We propose that each ACC_n solves this through an iterative negotiation process among the dispatchable agents within this ACC. This is proposed to be carried out by the faster timescales, $k \in \{1, \ldots, k^{*}\}$ for each j, that is, at each forecast instance j, the negotiation process starts at $k = 0$, where $\hat{P}_j^{\text{re}}$, $\hat{P}_j^{e}$, $\hat{P}_j^{\text{th}}$, and $\hat{P}_j^{T}$ are fixed, allowing the railway operator at ACC_n to establish the electric and thermal loads for the dispatch horizon. Also, at $k = 0$, it is assumed that the railway operator for ACC_n broadcasts an initial price duple $\lambda_{n,j,k=0} = [\lambda_{n,j,0}^{e}, \lambda_{n,j,0}^{\text{th}}] \in \mathbb{R}^M$ consisting of electric and thermal prices.

With these initial conditions, using a Lagrangian and a gradient-based update, the decision variables $y_{i,j}^{k} \in \mathbb{R}^M$ and the prices $\lambda_{n,j,k}^{e} \in \mathbb{R}^M$ and $\lambda_{n,j,k}^{\text{th}} \in \mathbb{R}^M$ are updated at each negotiation instance k as

$$y_{i,j}^{k+1} = y_{i,j}^{k} - \beta_{y_i}\Big(\nabla_{y_{i,j}^{k}} J_i(y_{i,j}^{k}) + \left[\nabla_{y_{i,j}^{k}} h^{e}\right]^{T} \lambda_{n,j,k}^{e} - \left[\nabla_{y_{i,j}^{k}} h^{\text{th}}\right]^{T} \lambda_{n,j,0}^{\text{th}} \mp \mu_{i,j}^{\pm k}\Big) \tag{22}$$

$$\lambda_{n,j,k+1}^{e} = \lambda_{n,j,k}^{e} + \beta_{\lambda^e}\left(\hat{P}_j^{\text{re}} + \hat{P}_j^{T} + \hat{P}_j^{e} + \sum_{i \in \mathcal{A}_n} g_i^{e}\left(y_{i,j}^{k}\right)\right) \tag{23}$$

$$\lambda_{n,j,k+1}^{\text{th}} = \lambda_{n,j,k}^{\text{th}} + \beta_{\lambda^{\text{th}}}\left(\hat{P}_j^{\text{th}} + \sum_{i \in \mathcal{A}_n} g_i^{\text{th}}\left(y_{i,j}^{k}\right)\right) \tag{24}$$

where $\beta_{y_i}, \beta_{\lambda^e}, \beta_{\lambda^{\text{th}}} \in \mathbb{R}\ \forall\ i \in \mathcal{A}_n$ are positive step-size parameters and $\mu_{i,j}^{\pm} \in \mathbb{R}\ \forall\ i \in \mathcal{A}_n$ is the penalty for violating capacity constraints (20) and (21). The penalty function

updates are given by

$$\mu_{i,j}^{\pm k+1} = \max\{0\ ,\ \mu_{i,j}^{\pm k} + \beta_{\mu_i}\mu_{i,j}^{\pm k}\} \tag{25}$$

where β_{μ_i} is a positive step-size parameter.

It is assumed that these iterations occur at each k and converge as $k \to k^*$ for some k^*. As outlined in [14], under suitable convexity conditions, it can be shown that convergence to unique optimal values takes place.

Defining $\hat{P}_j^F = [\hat{P}_j^{\text{re}} + \hat{P}_j^e, \hat{P}_j^{\text{th}}]$ as the estimate of the fixed assets at j, these estimates can be updated with j as the new forecasts arrive. The forecast update enables an improved dispatch of the agents across the dispatch intervals $K \in \{1, \ldots, M\}$. Note that in practice, exit conditions based on the agent output and price profile updates within the negotiation process can be established such that the forecast update is promptly initiated. These exist conditions follow the form: $|y_{i,j}^{k+1} - y_{i,j}^k| \leq \gamma_k^{\ y}$ & $|\lambda_{n,k+1,j} - \lambda_{n,k,j}| \leq \gamma_k^{\lambda}$. If these conditions are met, the equilibrium agent output and price profiles can be set as $y_{i,j}^* = y_{i,j}^{k+1} \forall i \in \mathcal{A}_n$ and $\lambda_{n,j}^* = \lambda_{n,k+1,j}$, respectively.

Similarly, exit conditions can be established for the forecast update process such that the agent output and price profile updates can be communicated for dispatch and settlement if so desired. These exit conditions follow the form: $|y_{i,j+1}^* - y_{i,j}^*| \leq \gamma_j^{\ y}$ & $|\lambda_{n,j+1}^* - \lambda_{n,j}^*| \leq \gamma_j^{\lambda}$. If these conditions are met, dispatch for the first interval $K = 1$ can be established using agent output profiles $y_i^{**} = y_{i,j+1}^* \forall i \in \mathcal{A}_n$ and price profiles $\lambda_n^{**} = \lambda_{n,j+1}^*$.

In summary, the railway dispatch algorithm for $K = 1$ starts at $k = 1, j = 1$ with a forecast of the power profile for each renewable generator, $\hat{P}_j^{\text{re}} \in \mathbb{R}^M$, electric load, $\hat{P}_j^e \in \mathbb{R}^M$, thermal load, $\hat{P}_j^{\text{th}} \in \mathbb{R}^M$, and the total traction load, $\hat{P}_j^T \in \mathbb{R}^M$, and returns the optimal agent output profiles y_i^{**}, the total traction demand profile P^{T**} and the price profiles λ_n^{**} that can be used for dispatch and settlement of dispatch interval $K = 1$. The dispatch interval window then shifts over, with $K = 2$ corresponding to the active dispatch interval and the process repeats.

IV. Train Dispatch

In Section III, we assumed that at each ACC_n, the train loads $\mathcal{T}_n$ were fixed and the dispatch of the active agents A_n was optimized. In this section, we address the fact that these train loads are indeed flexible and pose a constrained optimization problem for determining the optimal profiles of power generation and consumption. In Section IV-A, we describe the physical model of the train. Next, we define the cost minimization problem for a track with multiple pricing regions, managed by ACC_n in Section IV-B. With this train dispatch accomplished, in Section V, we describe how the railway dispatch optimization described in Section III can be stitched together with the train dispatch optimization to result in an overall transactive control framework for the combined grid-railway infrastructure. This overall framework is validated using numerical simulation of the Amtrak NEC in Section VI.

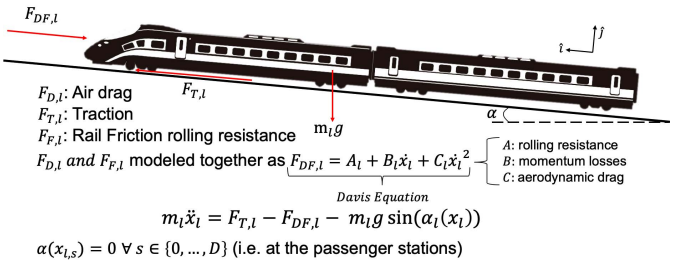

Fig. 3. Free body diagram of electric train l. The resulting traction force $F_{T,l}$, the friction and drag force $F_{\text{DF},l}$, and the gravitational force component in the direction of motion of the train $m_l g \sin \alpha_l(x_l)$ are identified. Newton's second law of motion is written for the $\hat{\mathbf{i}}$-direction, along the direction of motion of the train.

A. Dynamic Model of Electric Trains

The power consumption of the electric train depends on the traction force, which in turn depends on the overall train dynamics. In this section, we derive the underlying dynamic model of the train and the corresponding power consumption profile. The position, velocity, and acceleration of train l in the direction of motion $\hat{\mathbf{i}}$ are denoted by x_l, $\dot{x}_l$, and $\ddot{x}_l$, respectively. We proceed by defining the three forces with a component in the direction of motion of the train $\hat{\mathbf{i}}$ as it travels at an angle $\alpha_l(x_l)$ from the horizon (see Fig. 3). The gravitational force on the train can be decomposed into the direction of motion $\hat{\mathbf{i}}$ as $-m_l g \sin(\alpha_l(x_l))$ and the direction normal to the ground $\hat{\mathbf{j}}$ as $-m_l g \cos(\alpha_l(x_l))$, where m_l is the total mass of the train. The electric motors converting electrical into mechanical power are assumed to result in the traction force $F_{T,l}$ in the $\hat{\mathbf{i}}$-direction. An opposing force $F_{\text{DF},l}$ is also included in the model, which includes a drag force and a friction force [22]. With these definitions, we can derive the equation of motion in the direction of motion $\hat{\mathbf{i}}$ as

$$m_l\ddot{x}_l = F_{T,l} - F_{\text{DF},l} - m_l g \sin \alpha_l(x_l). \tag{26}$$

The traction force $F_{T,l}$ is a function of both the electric power P_l and $\dot{x}_l$ and is in general a mapping of the ratio $P_l/\dot{x}_l$. The drag–friction force can be represented as

$$\sum F_{\text{DF},l} = A_l + B_l\dot{x}_l + C_l\dot{x}_l^2 \tag{27}$$

known as Davis equation [22]. This industry standard approximation captures the rolling resistance effect at low speed through the linear term and the drag force through the quadratic term. More detailed drag–friction models for train cars can be found in [23].

B. Constrained Optimization Problem

Before stating the optimization problem, a few notations and details related to the train trajectories are addressed. Let us assume that train l departs location x_0 at time t_0 and arrives at a final destination x_f at time t_f. Let us assume that the train stops at passenger stations denoted by $s \in \{0, \ldots, D\}$ between $t \in [t_{l,a}(s), t_{l,d}(s)]$, where $t_{l,a}(s)$ and $t_{l,d}(s)$ are the arrival and departure times, respectively, from station s and $x_{l,s}$ denotes the position of station s. Over the period $[t_0, t_f]$, the train is assumed to traverse n subsections, each dispatched

by ACC_n, with the travel during the time interval $[t_{l,n-1}, t_n]$ that corresponds to a position interval $[x_{n-1}, x_n]$, and not necessarily coincident with the station locations. Let us denote the corresponding power-demand profile for this train as

$$P_l(t) = \begin{cases} P_l(t,1), & t \in [t_{l,0}, t_{l,1}] \\ \quad\vdots & \\ P_l(t,N), & t \in [t_{l,N-1}, t_{l,N}]. \end{cases} \tag{28}$$

We assume that the railway is level at the passenger stations (i.e., $\alpha(x_{l,s}) = 0, \forall\ s \in \{0,\ldots,D\}$) implying that the power demand of the train during the stop is equal to zero, $P_l(t) = 0 \in [t_{l,a}(s), t_{l,d}(s)], \forall\ s \in \{0,\ldots,D\}$.

During the same time intervals, the train operator l faces prices $\lambda_l(t,n), \forall\ t \in [t_{l,n-1}, t_{l,n}], \forall\ n \in \{1,\ldots,N\}$, summarized as

$$\lambda_l(t) = \begin{cases} \lambda_l(t,1), & t \in [t_{l,0}, t_{l,1}] \\ \quad\vdots & \\ \lambda_l(t,N), & t \in [t_{l,N-1}, t_{l,N}]. \end{cases} \tag{29}$$

We determine the prices $\lambda_l(t)$ from the price profiles λ_n^{**} determined in Section III as follows. Suppose that the time interval $[t_{l,n-1}, t_{l,n}]$ is specified, which corresponds to the time interval over which train l traverses ACC_n. We choose an arbitrary time $t_K \in [t_{l,n}, t_{l,n+1}]$, and suppose that it corresponds to the Kth interval (e.g., the time horizon corresponds to $K = 1$ in the example shown in Fig. 2). Then, $\lambda_l(t,n)$ corresponds to the Kth element of $\lambda_n^{e**} \in \mathbb{R}^M$. The same process is repeated for all $n = 0,\ldots,N$.

With the above definitions in place, the train dispatch problem, which corresponds to the optimal profiles of generation and consumption of power corresponding to each train, is now posed. Assuming that $\lambda_l(t)$, defined in (29), is determined using the railway dispatch algorithm in Section III-C, the train power profiles are determined through the minimization of the energy cost of train l as

$$\min_{x_l, \dot{x}_l} \int_{t_0}^{t_f} P_l(\psi)\lambda_l(\psi)d\psi \tag{30}$$

$$\text{s.t. } m_l\ddot{x}_l + F_{\text{DF},l}(\dot{x}_l) + m_l g\sin(\alpha_l(x_l)) = F_{T,l}\left(\frac{P_l}{\dot{x}_l}\right) \tag{31}$$

$$\underline{P_l}(x_l) \le P_l \le \overline{P_l}(x_l) \tag{32}$$

$$\underline{F_{T,l}}(\dot{x}_l) \le F_{T,l} \le \overline{F_{T,l}}(\dot{x}_l) \tag{33}$$

$$\underline{a_l} \le \ddot{x}_l \le \overline{a_l} \tag{34}$$

$$\underline{v_l}(x_l) \le \dot{x}_l \le \overline{v_l}(x_l) \tag{35}$$

$$t_{l,a}(s) \ge \underline{t_l}(s), \quad s \in \{0,\ldots,D\} \tag{36}$$

$$t_{l,d}(s) \le \overline{t_l}(s), \quad s \in \{0,\ldots,D\} \ge B_F. \tag{37}$$

In the above, (30) represents the total energy cost incurred by train l over $[t_0, t_n]$. Equation (31) corresponds to the train kinematics, which includes the dependence of the traction force on the power profile as well as the train velocity. Inequalities (32)–(37) denote various constraints on power, force, velocity, acceleration, and times that need to be accommodated. Limits in (33) are determined by the traction force curve of the train manufacturer, and limits in (34) and (35) correspond to safety considerations and civil speed limit restrictions in densely populated areas. Limits in (36) and (37) correspond to schedule constraints. The optimization problem in (30)–(37) continues being nonlinear and nonconvex due to the fact that $P_l(t)$ in (30) is a highly nonlinear function of the decision variables $(x_l, \dot{x}_l)$, as it depends on the traction force and therefore $\ddot{x}_l$. It should be noted that all the time intervals $[t_{l,i}, t_{l,i+1}]$ also depend on the decision variables, which adds to the nonlinearity as well. However, the crucial difference between the solution of this problem and the overall problem stated in Section II is the decoupling of the prices from the decision variables $(x_l, \dot{x}_l)$ and, therefore, the time instants $t_{l,i}$. As the prices in turn are determined from both a gridwise and a railwaywise perspective as outlined in Section III, decoupling them from this optimization problem as outlined above simplifies the problem significantly. In particular, as outlined above, the price profiles $\lambda_l(t)$ can be determined using the railway dispatch algorithm for a given time interval, and the time interval in turn is determined using the optimization procedure of the train dispatch outlined here in this section in (30)–(37). It is decoupling into these two separate dispatch problems that represent the main contribution of this article.

The solution of the train dispatch problem in (30)–(37) can be determined using any one of several commercial software packages such as MATLAB's fmincon [24]. Numerical solvers need to be employed to transform the continuous variables (including the decision variables) to discrete-time variables of length $(t_f - t_0)\delta\psi$, where $\delta\psi$ is the time step.

V. Overall Transactive Control Architecture—rDMM

In Section II, we posed a combined optimization problem of railway dispatch and train dispatch in the form of (1)–(10). In order to make the problem more tractable, we divided it into two steps, which were addressed in Sections III and IV. In Section III, we presented a constrained optimization problem that solves for the optimal dispatch of energy assets, where loads, including those of trains as well as renewable generation, were assumed to be fixed and the electric and thermal schedules and prices for the generators along the track are determined as $[g_i^e(y_i^{**}), g_i^{\text{th}}(y_i^{**})] \in \mathbb{R}^M$ and $\lambda_n^{**} = [\lambda_n^{e**}, \lambda_n^{\text{th}**}] \in \mathbb{R}^M$, respectively, for dispatch intervals $K \in \{1,\ldots,M\}$ in (17)–(21). This formulation captures the agent operational cost in the first term of (1) and ensures that the agent constraints (2)–(4) are met. In Section IV, we focused on the optimization of the train power consumption profiles themselves. In particular, we showed how each train operator can solve a constrained optimization problem in (30)–(37) to minimize energy costs given the track prices and required schedule. Minimizing the sum of trains' energy costs is equivalent to the second term of (1), subject to the constraints (5)–(10) for each train.

In this section, we summarize how the results of Sections III and IV can be interleaved to solve the combined optimization problem posed initially in Section II. This is accomplished by adjusting the power demand of the trains as a function of the prices from the railway dispatch problem, as a form of

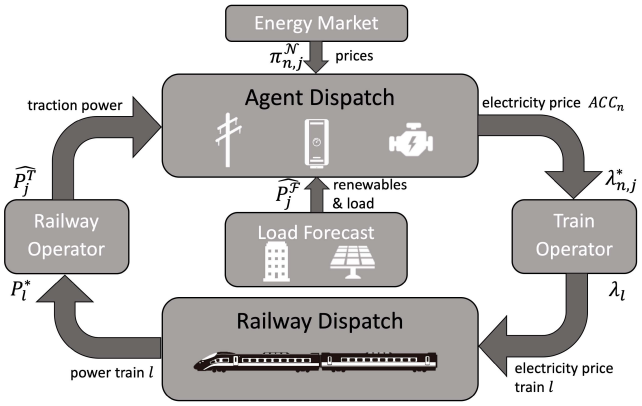

Fig. 4. Process flow of the two-step rDMM optimization, including railway dispatch and train dispatch. The train and railway operators are shown as the intermediaries between the problems that are being solved. Note that train operators and railway operators interact in a similar fashion with a growing number of ACC_n, $\forall n \in \{1, \ldots, N\}$, and trains $l \in \{1, \ldots, L\}$.

automated demand response at fast timescale, also referred to as transactive control [25], [26]. This transactive control-based ACC_n price provides an incentive for the electric trains to modify their dispatch by iteratively solving the cost minimization problem (30)–(37) with the updated prices. In what follows, we describe the overall transactive control architecture (see Fig.4 for an overall schematic and Algorithm 1 for details).

The top block in Fig. 4 denotes the agent dispatch and corresponds to the following functionality: at each forecast instance $j \in \{1, \ldots, j^{**}\}$, the agent dispatch block takes as inputs the traction power demand $\hat{P}_j^T$, passive agent output curves $\hat{P}_j^{\mathcal{F}}$, and the energy prices from the low-voltage-side network connections $\pi_{n,j}^{\mathcal{N}}$ and returns the price profiles $\lambda_{n,j}^*$ and the railway dispatch profiles $y_{i,j}^*$. As mentioned in Section III, the energy prices from the low-voltage-side network connections are used to determine the quadratic cost curve of these agents as in (14). Next, these cost curves are used to update the objective function (17) and the traction and passive agent output curves are used to update constraints (18) and (19). The iterative dynamics in (17)–(21) are solved using (22)–(25) for negotiation instances $k \in \{1, \ldots, k^*\}$, stopping when the negotiation exit conditions defined earlier in Section III are met at each ACC_n.

The block on the right in Fig. 4 corresponds to the functionality of the train operator, who composes the price of energy profile for each train $l \in 1, \ldots, L$ in (29) using the electricity portion of the price profiles from the agent dispatch block, by determining the corresponding dispatch interval K and the corresponding element of the price vector λ_n^{e**}. These are then used in the train dispatch block (bottom) to determine the next dispatch profile forecast for each train P_l^*.

The bottom block in Fig. 4 denotes the train dispatch and uses the prices $\lambda_l(t)$ as in (29) to determine the cost-minimizing train dispatch for every train. This is accomplished using the optimization procedure discussed in Section IV: the energy price profiles from the agent dispatch block are used to update the objective function of the train dispatch problem in (30). Once this update is complete, a new power-demand profile of the train P_l^* is determined by solving (30)–(37).

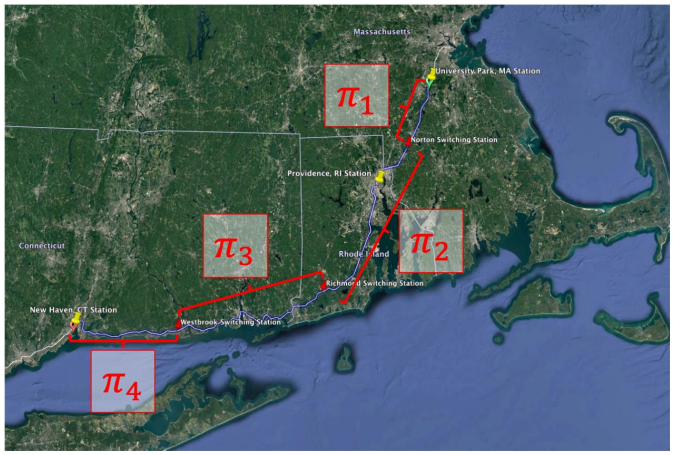

Fig. 5. Map of the four pricing regions identified along Amtrak's NEC between University Park Station in MA and New Haven Station in CT. This graphic and the road slope profile, $\alpha_l(x_l)$, used in simulation were developed using Google Earth Pro [27] and the data collected using the GPS of a mobile phone and the MyTracks iOS application [28].

The block on the left in Fig. 4 represents the railway operator, who collects the new power-demand profiles for each of the trains $l \in 1, \ldots, L$ after each forecast instance j and assembles the total traction power demand for each ACC in (16). This new profile is used in the negotiations (22)–(25), in addition to new forecasts that may become available from other passive agents $\hat{P}_j^F = [\hat{P}_j^{\text{re}} + \hat{P}_j^e, \hat{P}_j^{\text{th}}]$ at each j and energy prices from the low-voltage-side network connections $\pi_{n,j}^{\mathcal{N}}$ used to determine the cost function parameters $a_{i,K}$, $b_{i,K}$, and $c_{i,K}$ in (14) for $i \in \mathcal{N}$.

The cycling between the agent dispatch and train dispatch blocks repeats for forecast instances $j \in \{1, \ldots, j^{**}\}$. If the resulting price $\lambda_{n,j}^*$ and railway dispatch $y_{i,j}^*$ profiles meet the forecast exit conditions for the network ($|y_{i,j+1}^* - y_{i,j}^*| \geq \gamma_j^y$ & $|\lambda_{n,j+1}^* - \lambda_{n,j}^*| \geq \gamma_j^\lambda$), then the algorithm stops, dispatching the agents at the last negotiation equilibrium y_i^{**}, and is compensated based on the price profiles λ_n^{**} from the top block. Similarly, trains are dispatched based on the last forecast update P^{T**} from the bottom block and train operators are required to pay the last negotiation equilibrium price λ_n^{**}. As mentioned before, the overall iteration is ensured to stop by using suitable exit conditions. A settlement procedure may be designed to collect the payments of the agents at a slower frequency than the convergence of the rDMM (i.e., monthly payments). Once dispatch takes place for $K = 1$, the dispatch horizon shifts by one interval, and the procedure set forth with $j = 1$ starts again.

VI. Simulations

A. Methods and Parameters

The northern Amtrak NEC between Boston, MA, and New Haven, CT (within the ISO-NE power system), emerges from a review of the electric railway systems in USA as a prime case study for our analysis, due to its four segmented rail power zones that result in the pricing regions identified in Fig. 5. The four ACCs, ACC_n identified with $n \in \{1, 2, 3, 4\}$, are powered by the substations at Sharon, MA; New Warwick, RI; London, CT; and Branford, CT, and are considered separate pricing regions, each with price $\pi_n \forall n \in \{1, 2, 3, 4\}$ (see Fig. 6).

Algorithm 1 rDMM

Train Inputs: $m_l, F_{DF,l}, \alpha_l, F_{T,l}, \underline{P_l}, \overline{P_l}, \underline{F_{T,l}}, \overline{F_{T,l}}, \underline{a_l}, \overline{a_l}, \underline{v_l}, \overline{v_l}, \underline{t_l}(s), \overline{t_l}(s)\ \forall l \in \{1,\ldots,L\}, s \in \{0,\ldots,\overline{D}\}$

Agent Inputs: $\underline{P_i^e}, \overline{P_i^e}, \underline{P_i^{th}}, \overline{P_i^{th}}, J_i(y_i), \hat{P}_j^{\mathcal{F}_n}, \pi_{n,j}^{\mathcal{N}} \forall i \in \mathcal{A}_n$

$j = 1$; $\lambda_{n,0} = 0$
{Dispatch Interval $K = 1$}
while $\left|y_{i,j}^* - y_{i,j-1}^*\right| > \gamma_j^y$ *OR* $\left|\lambda_{n,j}^* - \lambda_{n,j-1}^*\right| > \gamma_j^\lambda$ **do**
  for $l \in \{1,\ldots,L\}$ **do**
    Update (29) using $\lambda_{n,j}^*$
    Solve (30)-(37) for P_l^* {Train Dispatch}
  end for
  {Forecast instance update across each ACC_n}
  for $n \in \{1,\ldots,N\}$ **do**
    Update (16) using $P_l^*\ \forall\ l\ \in\ \{1,\ldots,L\}$
    Update (17)-(19) using $\hat{P}_j^T$, $\hat{P}_j^{\mathcal{F}_n}$, $\pi_{n,j}^{\mathcal{N}}$
    $k = 0$
    {Agent negotiation}
    while $|\lambda_{n,k+1} - \lambda_{n,k}| > \gamma_k$ **do**
      Solve for y_i^{k+1} in (22)
      Solve for $\lambda_{n,k+1}^e$ in (23) and $\lambda_{n,k+1}^{th}$ in (24)
      $k++$
    end while
    Update $\lambda_{n,j} = \lambda_{n,j+1}$ and $\lambda_{n,j+1} = \lambda_{n,k^*}$
  end for
  $j++$
end while
Dispatch λ_n^{**}, y_i^{**}, P^{T**} for $K = 1$.

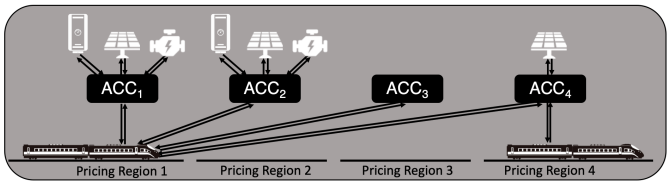

Fig. 6. Schematic of the ACCs proposed for Amtrak's Northend NEC used in the simulation. The four ACCs have varying levels of load, renewable deployment, dispatchable agents, and network energy pricing.

Using the location of these substations, publicly available electric utility tariff information [29], [30], [31] and real-time energy market data from ISO-NE [32], we estimate the total energy cost to the operator (composed of supply and delivery charges) at each one of the four ACC_n's which are in turn used as the low-voltage side network connection costs $\pi_{n,j}^{\mathcal{N}}$ of the four network connection agents $\mathcal{N}_n$ that are used to update the quadratic cost curve of these agents in (15). Based on the characteristics of the Route 128/University Park (ACC_1) and Providence (ACC_2) passenger stations and their surrounding commercial spaces, we also add cogeneration assets $\mathcal{C}_n$ and boilers $\mathcal{H}_n$ using NREL's system advisory model (SAM) [33] for thermal ($\underline{P_i^{\text{th}}}$, $\overline{P_i^{\text{th}}}$) and electric ($\underline{P_i^e}$, $\overline{P_i^e}$) sizing, and estimation of the quadratic cost function coefficients in (15), as summarized in Table I.

Due to the large roofs and parking lots near the University Park, Providence, and New Haven passenger stations, we also assumed that three PV solar arrays re_n can be added at ACC_1, ACC_2, and ACC_4 and used SAM alongside satellite imagery to size the arrays and estimate their production, $\hat{P}_j^{\text{re}_n}$. We also used the satellite imagery to measure the footprint of the passenger stations and estimate the electric ($\hat{P}_j^{e_n}$) and thermal ($\hat{P}_j^{\text{th}_n}$) load using the EPA commercial building templates that can be accessed through SAM.

Amtrak's high-speed Acela Express service along the NEC utilizes high-speed locomotives developed by Bombardier in the late 1990s based on the French TGV [34]. Acela Express trains have a total empty weight of 531.2 MT and a full capacity weight of 556.7 MT. In simulation, we assume a partially occupied weight of $m_l = 545$ MT. Although the Acela trains are designed to achieve a 264-km/h top speed, they are limited in operation to 240 km/h, which is equivalent to $\overline{v_l} = 66.67$ m/s.

The maximum train traction power $\overline{P_l}$ is 9.2 MW, while regenerative braking is limited in operation to $\underline{P_l} = -6.0$ MW [1]. In the absence of public data on the acceleration rates of high-speed trains such as the Acela, the estimates used in our simulation ($\underline{a_l} = -0.5$ ms^{-2} and $\overline{a_l} = 0.5$ ms^{-2}) were adopted from models of electric train systems used by EPRail. Fitting the Davis equation (27) to the Acela Express drag and rail friction curve, $F_{\text{DF},l}$, we have that $A_l = 10,195.16$, $B_l = 65.81$, and $C_l = 25.02$.

Using the pricing information of the nodes along the track and the Amtrak Acela Express train timetable [35] as departure ($\overline{t_l}(s)$) and arrival ($\underline{t_l}(s)$) times for each station, we simulate a train following a power profile that minimizes total work as a baseline and a train dispatched by the rDMM methodology summarized in Algorithm 1.

B. Results

We now report the results obtained using the rDMM outlined in Section V, which we will denote as the transactive controller. In particular, Algorithm 1 was run with all numerical parameters, as shown in Table I. The results of the rDMM are shown in Figs. 7 and 8 for a single train's travel profile corresponding to the 6:21 A.M. University Park departure of Acela 2155 on January 18, 2018, a day that exhibited large network pricing differentials. These figures depict the key decision variables of the rDMM. Fig. 7 include the energy price λ_n^{**} and the power consumption P_l^* as the train traverses the four ACCs. Fig. 8 includes other key decision variables corresponding to the same run, which are position x_l and velocity $\dot{x_l}$ for the single train. It can be seen that the train schedules are met, and the velocity limits are accommodated. The most interesting result corresponds to the energy price shown in the top plot in Fig. 7 and corresponds to the minimization of the cost function in (17). This price profile in turn leads to an optimized cost in (30) of U.S. $200.62 for this single train travel.

C. Discussion

We now make some observations based on the results obtained above. We evaluate the optimality of the proposed transactive architecture, through a comparison with two other

TABLE I

AGENT NUMERICAL PARAMETERS USED IN SIMULATION. MAXIMUM CAPACITY IS EXPRESSED FOR THE BINDING THERMAL OR ELECTRIC CHARACTERISTIC AND CAN BE IDENTIFIED BY THE MAPPING COEFFICIENT d_i^e OR d_i^{TH} THAT IS EQUAL TO 1. THE OTHER COST FUNCTION PARAMETERS IN (14) WERE USED AT A MINIMUM IN SIMULATION, SETTING c_i TO A SMALL POSITIVE QUANTITY

ACC_n	Agent	$\overline{P_i^{e,th}}$	d_i^e	d_i^{th}	$b_{i,K}$
1	$\mathcal{H}_1$	10,432	0	1	0.0303
1	$\mathcal{C}_1$	1,550	1	1.02	0.0629
1	$\mathcal{N}_1$	10,000	1	0	$\pi_{1,j}$
2	$\mathcal{H}_2$	20,864	0	1	0.0303
2	$\mathcal{C}_2$	4,560	1	2	0.0818
2	$\mathcal{N}_2$	10,000	1	0	$\pi_{2,j}$
3	$\mathcal{N}_3$	10,000	1	0	$\pi_{3,j}$
4	$\mathcal{N}_4$	10,000	1	0	$\pi_{4,j}$

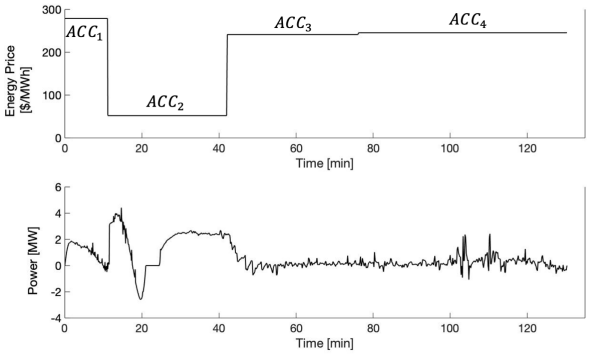

Fig. 7. Plot of average energy price ($/MWh) of a southbound trip on Amtrak Acela between University Park Station in MA and New Haven Station in CT with a stop in Providence Station in RI. The power trajectory (MW) for the train dispatched by the rDMM methodology is also plotted on the price plot, showcasing the power injection from the train into the electric railway during regenerative braking.

train profiles that are shown in Fig. 8. The first one corresponds to a field dataset that was collected using the GPS of a mobile phone and the MyTracks iOS application [28] on the Acela 2171. It can be seen that the maximum speed of 66.7 m/s as well as the position datasets corresponding to the transactive controller are consistent with our field dataset. We computed the corresponding train cost for this field dataset assuming the same dynamical model for the Acela train employed in simulation, summarized in (31), which allows us to solve for the traction force $F_{T,l}$ as a function of the position, velocity, and acceleration datasets collected with the phone GPS and accelerometers. This force dataset can in turn be used in conjunction with the volatility dataset to arrive at the tractive power profile for the route. Finally, the marginal cost along the route, set by the low-voltage-side network connection cost, can be applied to the profile to determine the total cost. It was observed that this cost was U.S. $865.01, which shows that our rDMM results in a 75% reduction. It is possible that the actual reduction from the rDMM may be somewhat smaller, as we

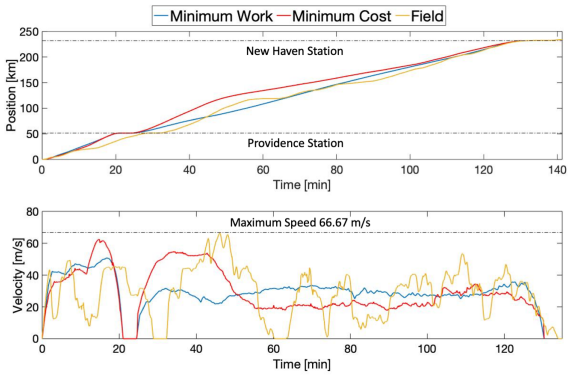

Fig. 8. Plots of position (km) and velocity (m/s) of a southbound trip on Amtrak Acela between University Park Station in MA and New Haven Station in CT with a stop in Providence Station in RI for a train that minimizes work (blue line), a train one dispatched following rDMM (red line), and a field train (yellow line).

have not incorporated other speed limit restrictions along the track such as rail crossings and densely populated areas in the simulation of the rDMM.

The second profile shown in Fig. 8, denoted as minimum work, was obtained by solving the train dispatch problem in (30)–(37) with a uniform price profile $\lambda_l(\tau) = 1$. This yielded a position and velocity profile, as shown in Fig. 8. The corresponding price profile is shown in Fig. 8 as well, which led to a total trip cost U.S. $273.69. Note that the train dispatched by the rDMM methodology can achieve a 25% cost reduction when compared to the train dispatched under the standard minimum work (from U.S. $273.69 to $205.62), providing an initial estimate of the value of incorporating dynamic, price-responsive train dispatch in the electric railway operation.

In summary, the numerical simulation of the proposed two-step optimization mechanism applied to a segment of the Southbound Amtrak service along the NEC resulted in a 25% reduction in energy costs when compared to a standard trip optimization based on minimum work and a 75% reduction in energy costs when compared to the train cost calculated using a field dataset. To our knowledge, the current procedure adopted by Amtrak for the train profile does not have such an optimization approach but rather allows train operators to accelerate and decelerate the train at their discretion with the supervision and intervention of the positive train control system. The approach in [8], implemented in freight locomotives, employ algorithms similar to the minimum work method reported above.

VII. CONCLUSION AND FUTURE WORKS

Electric trains are a major untapped source of demand-side flexibility in electricity networks. Our findings contribute to the evolution of transportation control systems devoted to work minimization toward higher level objectives such as the social welfare maximization of joint transportation-electric infrastructures. In particular, our proposed two-step optimization of railway dispatch of all DER agents along the train track followed by train dispatch, facilitated by coordinated operations of the railway operator and train operator, suggests that the inclusion of time and space varying pricing

information modifies the optimal power profiles of DERs and trains, yielding reductions in electricity costs for relatively small increases in work. Simulation studies of the Southbound Amtrak service along the NEC in USA shows a 25% reduction in energy costs when compared to standard trip optimization based on minimum work and a 75% reduction in energy costs when compared to the train cost calculated using a field dataset.

Fundamentally, the rDMM introduces transactive energy as an additional degree of freedom in the control of a system, capitalizing on technology advancement (e.g., communication cost reductions, GPS, and widespread adoption of regenerative braking) to bridge the objectives of individual agents (e.g., trains and DERs) with those of global infrastructure (e.g., traction system and wholesale energy markets), that is, through adjustments of incentives in the form of electricity prices, we were able to ensure a coordinated set of profiles for all DERs and trains.

This technology could further motivate the deployment of automation technologies in train systems, as the business case improves when factoring electrical cost reductions. We expect that our findings could be developed into a software package for train operators, similar to GE's trip optimizer technology that has been adopted by heavy haul train operators to decrease fuel use [8].

1) Demand Charge Management: Although our work is a step toward including the electric traction system's costs within the train dispatch problem, we only reflect energy-related costs ($/MWh). In reality, the railway operator will also incur demand or capacity charges ($/MW) from the utility or ISO. These charges can also be reduced, in principle, using a transactive control methodology where the incentive signal shifts and smooths the power profile of the individual trains such that a reduction in demand at the main interconnection (traction substation) is met. We considered including the demand charge component within the cost function of low-voltage-side network connections $\mathcal{N}_n$ as a second-order term, but this methodology did not appropriately capture the timescale (typically months) at which demand charges are evaluated. A means of achieving demand charge management is to update constraints within the optimization problem, modifying the minimum and maximum power limits $\underline{P_l}(x_l)$ and $\overline{P_l}(x_l)$ in (32).

2) Regulation and Reserve Market Participation: Similar to the research direction regarding demand charges, we would like to extend the services provided by the transactive control system to the electrical network beyond energy and onto products for frequency regulation and operational reserves. Practical limitations of providing these services as well as the incentive and compensation mechanisms remain to be explored.

3) Mass Transit Systems: Our analysis focused on the practical intricacies of high-speed rail systems. Although our simulations were based on the high-speed rail example in USA, the Amtrak Acela service, we are aware that other systems, such as the MBTA mass transit T service, also evidence discontinuities in energy price along their track and have strategic plans to add rail-side generation [36]. Extending our simulation work to mass transit systems would widen the applicability of our proposed transactive control architecture.

4) Stochastic Modeling: In this article, we have employed a deterministic approach and have focused on the complex, nonlinear relationship between key decision variables that change with space and time. An extension to consider a stochastic counterpart of the approach proposed, building from the agent dispatch component, which requires energy market price, renewable generation, and load forecast inputs at each forecast instance $j = \{1, \ldots, j^{**}\}$, as well as the railway dispatch component outputs (see Fig. 4).

ACKNOWLEDGMENT

Any opinions, findings, conclusions, or recommendations are those of the authors and do not necessarily reflect the views of the NSF.

REFERENCES

[1] J. Yu and M. B. Ercolino, "Measurement and analysis of acela express regenerative power recovery," in *Proc. ASME/IEEE Joint Rail Conf.*, Jan. 2007, pp. 241–248.

[2] R. Melton, "Pacific northwest smart grid demonstration project technology performance report volume 1: Technology performance," Pacific Northwest Nat. Lab., Richland, WA, USA, Tech. Rep. PNW-SGDP-TPR-Vol.1-Rev.1.0 and PNWD-4438, 2015, vol. 1.

[3] F. Schweppe, R. Tabors, J. Kirtley, H. Outhred, F. Pickel, and A. Cox, "Homeostatic utility control," *IEEE Trans. Power App. Syst.*, vol. PAS-99, no. 3, pp. 1151–1163, May 1980.

[4] Y. Wang, B. Ning, F. Cao, B. De Schutter, and T. J. J. van den Boom, "A survey on optimal trajectory planning for train operations," in *Proc. IEEE Int. Conf. Service Oper., Logistics Informat.*, Jul. 2011, pp. 589–594.

[5] Y. Wang *et al.*, *Optimal Trajectory Planning and Train Scheduling for Urban Rail Transit Systems*. Cham, Switzerland: Springer, 2016.

[6] E. Khmelnitsky, "On an optimal control problem of train operation," *IEEE Trans. Autom. Control*, vol. 45, no. 7, pp. 1257–1266, Jul. 2000.

[7] R. Franke, P. Terwiesch, and M. Meyer, "An algorithm for the optimal control of the driving of trains," in *Proc. 39th IEEE Conf. Decis. Control*, vol. 3, Dec. 2000, pp. 2123–2128.

[8] D. Eldredge and P. Houpt, "Trip optimizer for railroads," in *The Impact of Control Technology*, T. Samad and A. Annaswamy, Eds. Manhattan, NY, USA: IEEE Control Systems Society, 2011. [Online]. Available: http://www.ieeecss.org/sites/ieeecss.org/files/documents/IoCT-Part2-20TripOptimizer-LR.pdf

[9] *Global Energy Review 2020*, IEA, Paris, France, Apr. 2020. [Online]. Available: https://www.iea.org/reports/global-energy-review-2020

[10] *Tracking Energy Integration 2019*, IEA, Paris, France, 2019. [Online]. Available: https://www.iea.org/reports/tracking-energy-integration-2019

[11] A. K. Bejestani, A. Annaswamy, and T. Samad, "A hierarchical transactive control architecture for renewables integration in smart grids: Analytical modeling and stability," *IEEE Trans. Smart Grid*, vol. 5, no. 4, pp. 2054–2065, Jul. 2014.

[12] J. Knudsen, J. Hansen, and A. M. Annaswamy, "A dynamic market mechanism for the integration of renewables and demand response," *IEEE Trans. Control Syst. Technol.*, vol. 24, no. 3, pp. 940–955, May 2016.

[13] D. J. Shiltz and A. M. Annaswamy, "A practical integration of automatic generation control and demand response," in *Proc. Amer. Control Conf. (ACC)*, Jul. 2016, pp. 6785–6790.

[14] D. Shiltz, M. Cvetković, and A. M. Annaswamy, "An integrated dynamic market mechanism for real-time markets and frequency regulation," *IEEE Trans. Sustain. Energy*, vol. 7, no. 2, pp. 875–885, Apr. 2016.

[15] T. R Nudell, M. Brignone, M. Robba, A. Bonfiglio, F. Delfino, and A. Annaswamy, "A dynamic market mechanism for combined heat and power microgrid energy management," *IFAC-PapersOnLine*, vol. 50, no. 1, pp. 10033–10039, Jul. 2017.

[16] T. R. Nudell *et al.*, "Distributed control for polygeneration microgrids: A dynamic market mechanism approach," *Control Eng. Pract.*, vol. 121, Apr. 2022, Art. no. 105052. [Online]. Available: https://www.sciencedirect.com/science/article/pii/S0967066121002999

[17] D. D'Achiardi, E. Pilo, S. K. Mazumder, and A. M. Annaswamy, "Transactive control approach to trip optimization in electric railways," in *Proc. IEEE 58th Conf. Decis. Control (CDC)*, Dec. 2019, pp. 3260–3265.
[18] S. P. Sarma, S. K. Mazumder, and E. P. De La Fuente, "Cost-reducing optimization strategies of electrical trains," in *Proc. 4th IEEE Workshop Electron. Grid (eGRID)*, Nov. 2019.
[19] O. N. Manzagol, "Power marketers are increasing their share of U.S. retail electricity sales," U.S. Energy Inf. Agency (EIA), Washington, DC, USA, Tech. Rep., Jun. 2018. [Online]. Available: https://www.eia.gov/todayinenergy/detail.php?id=36415
[20] E. Stuart, P. H. Larsen, J. P. Carvallo, C. A. Goldman, and D. Gilligan, "U.S. energy service company (ESCO) industry: Recent market trends," Ernest Orlando Lawrence Berkeley Nat. Lab., Berkeley, CA, USA, Tech. Rep. LBNL-1006343, 2016.
[21] D. S. Kirschen and G. Strbac, *Fundamentals of Power System Economics*. Hoboken, NJ, USA: Wiley, 2004.
[22] W. J. Davis, *The Tractive Resistance of Electric Locomotives and Cars*. Boston, MA, USA: General Electric, 1926.
[23] W. W. Hay, *Railroad Engineering*, vol. 1. Hoboken, NJ, USA: Wiley, 1982.
[24] T.M., *MATLAB Optimization Toolbox*, MathWorks, Natick, MA, USA, 2014.
[25] F. C. Schweppe, M. C. Caramanis, R. D. Tabors, and R. E. Bohn, *Spot Pricing of Electricity*. Norwell, MA, USA: Kluwer, 1998.
[26] P. Huang *et al.*, "Analytics and transactive control design for the Pacific northwest smart grid demonstration project," in *Proc. 1st IEEE Int. Conf. Smart Grid Commun.*, Oct. 2010, pp. 449–454.
[27] G. LLC. *Google Earth Pro V 7.3.2.5491. Data SIO, NOAA, U.S. Navy, NGA, Gebco, Ldeo-Columbia, NSF. Image Landsat, Copernicus*. Accessed: Jan. 14, 2019. [Online]. Available: http://www.earth.google.com
[28] D. Stichling, *Mytracks—The GPS-Logger V 5.0.4*, Dirk Stichling, Paderborn, Germany, May 2018.
[29] Eversource. (2018). *2018 Summary of Eastern Massachusetts Electric Rates for Greater Boston Service Area*. [Online]. Available: https://www.eversource.com/content/docs/default-source/rates-tariffs/ema-greater-boston-rates.pdf
[30] N. Grid. (Aug. 2018) *Electric Propulstion Rate (X-01)*. [Online]. Available: https://www.nationalgridus.com/media/pdfs/billing-payments/tariffs/ri/x01_ripuc_2194.pdf
[31] E. Energy. (2018) *Electric Service Rate 58*. [Online]. Available: https://www.eversource.com/content/docs/default-source/rates-tariffs/rate-58-ct.pdf
[32] ISO New England. (Oct. 2017). *Pricing Reports: Final Real-Time Hourly LMPS*. [Online]. Available: https://www.iso-ne.com/isoexpress/web/reports/pricing/-/tree/lmps-rt-hourly-final
[33] National Renewable Energy Laboratory. (Oct. 2017). *System Advisor Model V*. Accessed: Sep. 5, 2017. [Online]. Available: https://sam.nrel.gov/content/downloads
[34] B. Transportation, *Bombardier High-Speed Trainsets*, Saint-Bruno, Quebec, QC, Canada, document J3V 6E6, Nov. 2001.
[35] Amtrak, *Amtrak System Timetable*, National Railroad Passenger Corporation, One Massachusetts Ave, Washington, DC, USA, Jun. 2018.
[36] M. Donaghy, "MBTA's energy management program," Massachusetts Bay Transp. Authority, Boston, MA, USA, Tech. Rep., Jan. 2015.

David D'Achiardi received the B.S. degree in mechanical engineering and economics and the M.S. degree in mechanical engineering from the Massachusetts Institute of Technology (MIT), Cambridge, MA, USA, in 2016 and 2019, respectively.

He was a Research Assistant with the Active-Adaptive Control Laboratory, Department of Mechanical Engineering, MIT. Prior to that, he worked as a Mechanical Design Engineer at Tesla's Gigafactory, Reno, NV, USA. His research interests include energy market design under high renewable power adoption and transactive control of electric railway systems with distributed energy resources.

Mr. D'Achiardi was a recipient of the 2017 Douglas and Sara Bailey Scholarship and the 2015 Carl G. Sontheimer Prize for Excellence in Innovation and Creativity in Design from the Department of Mechanical Engineering, MIT.

Anuradha M. Annaswamy (Life Fellow, IEEE) is the Founder and the Director of the Active-Adaptive Control Laboratory, Department of Mechanical Engineering, Massachusetts Institute of Technology (MIT), Cambridge, MA, USA. She is the author of a graduate textbook on adaptive control, the coeditor of two vision documents on smart grids and two editions of the Impact of Control Technology report, and the coauthor of two National Academy of Sciences, Engineering, and Medicine Committee reports related to electricity grids. Her research interests span adaptive control theory and its applications to aerospace, automotive, propulsion, energy systems, smart grids, and smart cities.

Prof. Annaswamy is a fellow of IFAC. She has received best paper awards (Axelby; CSM), the Distinguished Member and Distinguished Lecturer Awards from the IEEE Control Systems Society (CSS), and the Presidential Young Investigator Award from NSF. She was a recipient of the Distinguished Alumni Award from the Indian Institute of Science in 2021. She served as the President for CSS in 2020.

Sudip K. Mazumder (Fellow, IEEE) received the Ph.D. degree in electrical and computer engineering from Virginia Tech, Blacksburg, VA, USA, in 2001.

He has been a Professor with the University of Illinois at Chicago (UIC), Chicago, IL, USA, since 2001, and the President of NextWatt LLC, Hoffman Estates, IL, USA, since 2008. He has over 30 years of professional experience.

Dr. Mazumder has been a fellow of American Association for the Advancement of Science (AAAS) since 2020 for original contributions in power electronics controls. He served as a Distinguished Lecturer for IEEE from 2016 to 2019. He received UIC's Distinguished Researcher of the Year Award in 2020, the Inventor of the Year Award in 2014, and the University Scholar Award in 2013, and the IEEE TRANSACTIONS ON POWER ELECTRONICS Prize Paper Awards in 2022 and 2002. He was the Chair of the 2021 IEEE Power Electronics for Distributed Generation Conference. Since 2019, he been serving as the Editor-at-Large for IEEE TRANSACTIONS ON POWER ELECTRONICS, the leading journal in power electronics in the world.

Eduardo Pilo (Senior Member, IEEE) received the Ph.D. degree from the ICAI School of Engineering, Comillas Pontifical University, Madrid, Spain, in 2003.

From 2003 to 2010, he was a Researcher with Comillas Pontifical University. From 2010 to 2012, he worked for the electrical industry as a consultant of the company Multitest09. In 2012, he founded his own company, EPRail, focused on providing research and consultancy services in the field of power systems and railways. From June 2013 to July 2014, he was a Visiting Professor and a Research Scientist with the University of Illinois at Chicago, Chicago, IL, USA. Since May 2019, he serves as a full-time Professor with the Universidad Francisco de Vitoria, Madrid. He has coauthored more than 40 journal articles and conference papers and book chapters in this field.

Dr. Pilo received the 10th Talgo Prize for Technological Innovation in 2010.